Polyimide/Cellulose Acetate Core/Shell Electrospun Fibrous Membranes for Oil-water Separation

Wenjing Ma[1], Zhongfu Guo[1], Juntao Zhao[1], Qian Yu[3], Fang Wang[1], Jingquan Han[4], Hui Pan[1], Jianfeng Yao[1], Qilu Zhang[5], Sangram Keshari Samal[2,6], Stefaan C. De Smedt[1,2]* and Chaobo Huang[1]*

[1]College of Chemical Engineering, Jiangsu Key Lab of Biomass-based Green Fuels and Chemicals, Nanjing Forestry University (NFU), Nanjing, 210037 P. R. China

[2]Lab General Biochemistry & Physical Pharmacy, Department of Pharmaceutics, Ghent University, 259000, Belgium

[3] College of Chemistry, Chemical Engineering and Materials Science, Soochow University, Suzhou, 215123, P. R. China

[4]College of Material Science and Engineering, Nanjing Forestry University (NFU), Nanjing, 210037 P. R. China

[5]School of Material Science and Engineering, Xi' an jiaotong University, Xi' an, 710049 P. R. China

[6]Material Research center, Indian institute of Science, Bangalore. 560012, India

Email: Chaobo.Huang@njfu.edu.cn.

Abstract

In recent years, efficient, cost effective oil-water separation technologies are highly desired due to frequent oil spill accidents. To design fibrous membranes for efficient oil-water separation, 'flexible' polyamide acid (PAA), being polyamide acid with ether linkages in the backbone, and 'heavily' fluorinated polybenzoxazine (F-PB) were synthesized. Cellulose acetate (CA) and PAA were co-axially electrospun; the PAA core was then imidizated at high temperature to obtain core/shell structured CA/polyimide (PI) electrospun fibrous

membranes; subsequently the surface of the fibers was modified with F-PB，in the presence or in absence of silica nanoparticles (SNPs). The mechanical strength, surface wettability, chemical and thermal stability, and oil-water separation potential of thus obtained PI/CA fibrous membranes were evaluated. The membranes show a much higher critical tensile stress (130 MPa) and critical tensile strain (52%), when compared with CA fibrous membranes. Due to the use of the 'heavily' fluorinated polybenzoxazine, the membranes are superhydrophobic with a water contact angle of 162^{o} and an oil contact angle which approaches 0^{o}. Interestingly, the newly designed PI/CA/F-PB-1/SNP-4 membranes can effectively separate various oil-water mixtures, solely driven by gravity, with a high flux (3106.2 ± 100 $L \cdot m^{-2} \cdot h^{-1}$) and a high separation efficiency (> 99%) and thus possess great potential for oil–water separation.

Keywords: Electrospinning, nanofibers, oil-water separation, membranes, filtration

1. Introduction

Oil-water separation has become a worldwide challenge owing to both the increased amount of industrial oily wastewater, as well as frequent oil spill accidents (like the Deepwater Horizon Gulf of Mexico oil spill disaster in 2010)[1-6]. Therefore, low cost materials, which allow efficient separation of oil from oil-water mixtures is a growing demand[7-9]. Conventional oil-water separation methods, such as gravity separation[10], adsorption[11], sedimentation under centrifugal field[12], biological treatment[13] and electro-coagulation[14] are available for separation of oil-water mixtures. However, there are still some disadvantages associated with these conventional techniques such as high operation costs, low separation efficiency, easy corrosion and generation of secondary pollutants, which significantly limit their industry-wide applications[15]. Membrane-based separation is an attractive technique as it is cheap, energy-efficient and applicable broadly in a wide variety of industrial settings. In the process of oil-water separation, wettability of the separating membrane plays an important role. Therefore, designing and fabricating membrane based materials with an optimal wettability is a major goal[16-18]. Electrospinning is one of the most simple and versatile methods that can produce fibrous membranes composed of fibers with diameters ranging from a few nanometers

to micrometers[19-22]. Electrospun nanofiber membranes have unique and interesting features for oil-water separation such as high surface area to volume ratio, large porosity, interconnected pore structure, flexibility in surface functionalities and good water permeability which is attractive[23-27]. Hence, electrospun fibrous membranes were found to have high separation capacity, high selectivity and stable performance for oil-water separation applications. Electrospun fibrous membranes based on different polymers such as polystyrene (PS)[5, 28], poly (vinyl alcohol) (PVA)[29, 30], polyvinylidene difluoride (PVDF)[31, 32], cellulose acetate (CA)[33], cellulose triacetate (CTA)[34], and polysulfone (PSF)[35, 36] were reported so far for oil-water separation. Though, 'native' polymer electrospun membranes often do not meet the (practical) requirements for oil-water separation; to enhance the membranes' performance, modifications of the fibers, including the addition of other materials, is needed. For example, inorganic materials such as titanium dioxide (TiO_2) nanoparticles (NPs)[37, 38], silica NPs[39-43], sodium hydroxide (NaOH)[42], zeolite[44], MWCNTs[45], zirconia (ZrO_2)[46-48], zinc oxide (ZnO)[49, 50], and silver NPs[51] were incorporated into the polymeric matrices to form hybrid membranes.

In a recent study Shang et al[52] designed a superhydrophobic and superoleophilic fibrous membrane through a facile combination of electrospun CA nanofibers and an in situ polymerized F-PB functional layer in which silica nanoparticles (SNPs) were incorporated. Such fibrous membranes could effectively separate dichloromethane/water mixtures with high flux and separation efficiency via filtration. Similarly, Huang et al[53] prepared a superhydrophobic "TiO_2@fabric composite" which was highly stable against repeated abrasion and UV exposure and allowed highly efficient oil–water separation. In another study Wang et al[54] developed smart stimuli-responsive poly (N-isopropylacrylamide) (PNIPAAm)-modified regenerated cellulose (RC) fibrous membranes which are capable of switching oil/water wettability as a response to different temperatures. Such switchable surface wettability allowed controllable oil/water separation. However, most of the modified electrospun membranes remain fragile and highly sensitive to mechanical forces, which pose great restrictions on their industrial applications.

In the present study polyimide based polymers are under investigation. Such polymers possess good heat resistance, are corrosion resistant, chemically stable and show excellent mechanical properties; they are widely used in aviation, aerospace, electrical, micro electric automotive and other high-tech fields[55-60]. Cellulose acetate is an environment friendly, abundant raw material with good biocompatibility and biodegradability. In our previous study, we designed core-sheath structured PI/CA electrospun fibers[61]. The surface of these fibers was modified by fluorinated polybenzoxazine (F-PB) and SNPs. Our results demonstrated that such 'PI/CA/F-PB/SNP' membranes showed higher tensile strain (when compared to fibrous membranes composed of only CA), were hydrophobic and highly stable in a wide pH range. The membranes showed excellent gravity-driven oil-water separation features as well. The present work aims to overcome the remaining shortcomings of these membranes, namely their low tensile strain and poor flexibility which pose major restrictions on their industrial use[61]. Therefore, in the present study, 'flexible' polyamide acid, being polyamide acid with ether linkages in the backbone (Fig. 1) has been synthesized; the ether linkages are expected to act as flexible nodes thereby imparting the flexibility of the polymer chains. Furthermore, to make the surface of the fibers as hydrophobic as possible, 'heavily' fluorinated polybenzoxazine, has been synthesized (Fig. 2). We report on the elasticity, surface wettability, chemical and thermal stability, and oil-water separation potential of PI/CA membranes obtained with 'flexible' PAA and 'heavily' fluorinated polybenzoxazine.

2. Experimental section

2.1. Materials and reagents

Paraformaldehyde (POM), bisphenol AF, hexadecyl trimethyl ammonium bromide, hydrophobic silica (SiO_2) nanoparticles (7-40 nm), 4,4'-diaminodiphenyl ether (ODA) and p-phenylenediamine (PDA) were bought from Shanghai Aladdin Industrial Corporation. Cellulose acetate (Mw = 40 000 g/mol) was obtained from Sinopharm Chemical Reagent Co. Ltd. 2,5-Bis (trifluoromethyl) aniline (from Tianjin Heowns Biochemical Technology Co., Ltd). dichloromethane (DCM), *N, N*-Dimethylacetamide (DMAc), acetone, anhydrous calcium chloride, trichloromethane, sodium hydroxide and n-butyl acetate were purchased

from Nanjing Chemical Reagents Co. Ltd. 3,3',4,4'-Biphenyl tetracarboxylic diandhydride (BPDA) was purchased from TCI (Shanghai) development Co. Ltd., BPDA, PDA and ODA were sublimated under vacuum atmosphere using a sublimation setup (Synthware，Beijing, China) before using. All chemicals and solvents were reagent grade or the highest available commercial grade used as received without further purification，unless stated otherwise.

2.2. Synthesis of 2,2-bis (2, 5-Bis-trifluoromethylphenyl-l-3,4-dihydro-2H- 1,3-benzoxazinyl) propane (BAF-btfa)

For the synthesis of BAF-btfa. Paraformaldehyde (POM), bisphenol AF (BAF) and 2, 5-Bis (trifluoromethyl) aniline were used via the Mannich reaction, as shown in Fig. S1. A 250 mL round-bottom four-necked flask, equipped with a condenser and a thermometer, was loaded with 16.8115g bisphenol AF (BAF), 6 g paraformaldehyde and 22.912 g 2, 5-Bis (trifluoromethyl) aniline, was heated to 110 ^{o}C while vigorously stirring with an electric mixer under a nitrogen atmosphere. After refluxing for 24 h, the viscosity of reaction mixture was increased and reaction mixture was cooled to room temperature. The resulting solid reaction mixture was dissolved with trichloromethane（200 mL）and washed successively with 1.0% aqueous sodium hydroxide as well as deionized water. The solution was dried over anhydrous calcium chloride ($CaCl_2$) and, after removal of the drying agent, the solvent was removed by rotoevaporation. Subsequently the final product was dried in an oven at 60 ^{o}C under high vacuum for 24 h and slowly cooled down to room temperature to obtain BAF-btfa monomer powder. ^{1}HNMR spectrum (500 MHz, DMSO-d6), (500 MHz, $CDCl_3$) and ^{19}FNMR spectrum (500 MHz, $CDCl_3$) were recorded (see Fig. S2). The FTIR spectrum of prepared BAF-btfa is shown in Fig. S3.

2.3. Synthesis of polyamide acid (PAA)

We have obtained soluble polyamide acid (PAA) by the low-temperature solution polycondensation of BPDA with the mixtures ODA/PDA in DMAc (Fig. 1). The detail synthesis of PAA could be found in our previous work[18]. BPDA (2.9422 g) and ODA/PDA with varying molar ratios (10:0, 9:1, 8:2, 7:3, 6:4, 5:5, 4:6, 3:7, 2:8, 1:9, the total molar ratios of

dianhydride /diamine is 1/1) were successively introduced into a 100 mL three-necked round-bottomed flask equipped with a nitrogen inlet adapter, an electric mixer and a thermometer and partly immersed in a bath of alcohol under nitrogen atmosphere. Then 40 mL of DMAc was introduced slowly into the reaction mixture through a syringe. Note that the molar ratio BPDA/(ODA+PDA) was always one. By means of a thermostatic alcohol bath the mixture was cooled to -5°C and maintained at that temperature for 24 h. Then the reaction was terminated via exposing to air at room temperature and the molecular weight of the obtained PAA was characterized Gel Permeation Chromatography (GPC).

2.4. Electrospinning polyamide (PI) fibrous membrane

The electrospinning of PI was performed in a protocol described in our previous publication[18]. The as-prepared PAA was diluted with DMAc by vigorous stirring for 6 h to form 3 wt% precursor solution and small amount of hexadecyl trimethyl ammonium bromide (1 wt‰ to the weight of PAA) was added to the mixtures solution to increase the solution conductivity. Metal needle of 0.6 mm inner diameter was used for the electrospinning process. The electrospinning setup is shown in Fig. S4. An earthed rotational flywheel (30 cm in diameter) with speed of 1500 rpm was employed to collect the aligned fibers electrospun at a flow rate of 1.5 mL· h^{-1}. The distance between the needle tip and the ground collector was set as 10 cm and the positive voltage applied to polymer solutions was adjusted to 15 kV. The electrospinning process was carried out at room temperature. The resulted PAA membrane was studied by FT-IR spectrum analysis (see Fig. S1). The PI fibrous membranes were prepared with imidization post treatment of the PAA membranes under a temperature program of 150 ºC/1 h, 200 ºC /1 h, 250 ºC /1 h, 300 ºC /1 h, 350 ºC /3 h, 380 ºC/30 min.

2.5. Electrospinning of CA fibrous membranes

CA fibrous membranes were prepared according to the following procedure. Briefly, CA was dissolved with acetone and DCM mixture (25:75, v/v) in a water bath at 60 °C and the concentration of the solution was 7.5 % wt%. Subsequently, CA solution was loaded in a 1 mL plastic syringe equipped with a metal needle with a tip inner diameter of 0.68 mm and

injected through the needle at a controllable feeding rate of 3 mL/h. A positive voltage of 15 kV and negative voltage of 10 kV were applied to the needle to generate the CA jet. The collector distance between the needle tip and the collector was 15 cm. In order to collect aligned fibrous membranes, the resulting CA membranes were collected on the flywheel with rotating speed of 1500 rpm with 15 cm distance. The electrospun fibrous membrane were dried in a vacuum oven for 24 h to remove the solvents completely.

2.6. Coaxial electrospinning of PI/CA fibrous membranes

The basic schematic of experimental setup for co-axial electrospinning process was shown in Fig. S5. Briefly, it consisted of two syringe-like apparatus and a spinneret with an inner diameter of 0.51 mm needle coaxially placed inside an outer diameter of 1.2 mm one. The solution concentrations of PAA in DMAc (core) and CA in a mixed solvent of DCM/acetone (75:25 v/v) (shell) were 3 wt% and 7.5% w/v, respectively. The feed rate of the inner and outer dope was set at 0.5 and 1 $mL \cdot h^{-1}$, respectively. Both PAA and CA solutions were delivered via the coaxial needle with a programmable syringe pump. The distance between the needle tip and the collector was 13 cm and a 25 kV (+15, -10 kV) voltage was applied to the needle. A rotating roller (1500 rpm) controlled by a stepping motor as collector. All of the electrospun nanofibers were obtained in form of nonwoven sheets at ambient temperature of 25 °C with a relative humidity of 40% and were subsequently imidizated by annealing with temperature program of 150 ^{o}C /2 h, 200 ^{o}C /3 h, 250 ^{o}C /2 h and 260 ^{o}C /1 h.

2.7. Fabrication of F-PB/SNPs modified PI, CA and PI/CA fibrous membranes

Modify the CA, PI and PI/CA fibrous membranes was conducted by first immersing the electrospun fiber substrates into a 50 mL of BAF-btfa and SNPs n-butyl acetate solutions at room temperature and followed by stirred for 30 min. After the solvent evaporation spontaneous, the thus obtained membranes were dried in an oven for 2 h at 60 ^{o}C, then in situ polymerization of BAF-btfa monomers at temperature of 190-200 ^{o}C in vacuum atmosphere for 3 h. Finally, the membranes were rinsed using deionized water and stored for characterization. The BAF-btfa and SNPs concentration varied from 0.01% to 4% (w/w). The

membranes modified by using x wt% BAF-btfa/butyl acetate solutions and x wt% BAF-btfa/ y wt% SNPs/butyl acetate solutions were denoted as follows: CA/F-PB-x, PI/F-PB-x, PI/CA/F-PB-x, CA/F-PB-x/SNP-y, PI/F-PB-x/SNP-y and PI/CA/F-PB-x/SNP-y, respectively, here, x and y are the used concentrations of BAF-btfa (x wt%) and SNPs (y wt%), respectively.

2.8. Separation assessment

For oil-water separation, the as-prepared PI/CA/F-PB-1/SNP-4 fibrous membrane was fixed between the two glass funnels with effective separation area of 56.25×10^{-6} m^2 (Fig. 13a). A mixture of 10 mL of oil (dichloromethane (DCM)) colored with oil red and 10 mL of water colored with methyl blue was poured slowly into the upper test glass vessel through the as-prepared membrane and the separation was achieved, driven solely by gravity. Then the separated oil and water were collected with the beaker and the glass vessel, respectively.

The flux (F) of liquid through the membrane was calculated from the Equation. 1:

$$F = \frac{V}{A\Delta t} \quad (1)$$

Here, V (L) is defined as the volume of filtrated liquid, A (m^2) being the effective (surface) area of the separation membrane in the setup and Δt (h) is the filtration time.

The 'separation efficiency' (η) of liquid through the membrane was obtained according to the Equation. (2):

$$\eta = \frac{V_1}{V_0} \times 100 \quad (2)$$

Where, V_0 and V_1 are the volume of the water before and after the separation process, respectively.

2.9. The evaluation of porosity (P) of the fibrous membrane

The porosity (P) of the fibrous membrane was calculated according to the method of Liu's work [62].

$$\rho_{membrane} = \frac{mass_{membrane}}{area_{membrane} \times thickness_{membrane}} \quad (3)$$

$$\rho_{film} = \frac{mass_{film}}{area_{film} \times thickness_{film}} \quad (4)$$

$$P = \left(1 - \frac{\rho_{membrane}}{\rho_{film}}\right) \times 100\% \quad (5)$$

where $\rho_{membrane}$ and ρ_{film} are the density of the electrospun fibrous membrane and the corresponding manually deposited 'polymer film', respectively. Typically, the 'polymer film' was obtained by completely evaporating a 1.5 mL of 1wt% polymer solution that spread out homogeneously on a microscope glass plate and a micrometer screw gauge (Master proof, Germany) was used to assessed the thickness of the electrospun fibrous membrane and 'polymer film'.

2.10. Intrusion pressure (maxp)

The intrusion pressure (maxp) of the membranes was calculated using the following equation:

$$maxp = \rho g h_{max} \quad (6)$$

where ρ is the density of the water, g is acceleration of gravity, and h_{max} is the maximum height of water a PI/CA/F-PB-1/SNP-4 membrane can support.

2.11. Instrumentation

The fibrous membranes were fabricated using an FM1206 electrospinning apparatus (Beijing Future Material Sci-tech, China). Proton nuclear magnetic resonance (1H NMR) spectra were recorded by an AVANCE III HD 600MHz (Bruker Biospin). FT-IR spectra of the electrospun membranes were recorded at room temperature in a Nicolet 8700 FT-IR spectrometer, operating in the spectral between 2000 and 500 cm^{-1}. The surface morphologies, structure and diameters of the electrospinning nanofibers samples were determined with transmission electron microscope (TEM, JEM-1400, Jeol, Japan) and a field emission scanning electron

microscopy (FE-SEM, S-4800, Hitachi Ltd., Japan). The mechanical properties of the fibrous membranes were measured according to an UTM6502 electronic universal material testing machine (Shenzhen, China) at room temperature. The molecular weight of PAA was investigated using a gel permeation chromatography (GPC) (Agilent Technologies, Germany) equipped with one columns (Agilent, Plgel 5 μm, MIXED-C) and refractive index detector (Bryce) at 30 ºC. The elution phase was DMF (elution rate, 1 mL/min), and a series of polystyrene (PS) was used as the calibration standard. Thermogravimetric analyses of all samples were run on a Q5000-IR thermal gravimetric analyzer (TA Instruments) with samples sizes from 5 to 10 mg and held in platinum pans. All TGA experiments were performed under a nitrogen flow at a constant rate of 5 °C/min. The roughness parameters (Ra) of the membranes were determined by a white light interferometer (Contour GT-K, Bruker, USA). Contact angle of the samples were measured at five different regions of each surface and averaged on the same sample using a commercial JC2000D1 contact angle instrument (Shanghai, China) at 25 ºC. The Barrett–Jouner–Halenda (BJH) pore volume and pore size distributions (PSD) were obtained from the N_2 adsorption-desorption isotherms recorded at 393 K (Quantachrome, USA). The pore size distributions were analyzed with the adsorption branch data in the experiments. Finally, the oil concentration in the water fractions (obtained after separating the oil-water mixtures) was analyzed by a total organic carbon analyzer (Torch, USA).

3. Results and discussion

3.1. Mechanical properties of core/shell structured PI/CA nanofibers synthesized with flexible PAA

Fig. 3 shows the ‘critical tensile stress’ and ‘critical tensile strain’ (i.e. stress and strain at which the fibers break) of PI fibrous membranes obtained using PAA synthesized using various molar ratios of ODA and PDA. Clearly, the critical tensile strain of the fibrous PI membranes increased from 25% in case only PDA was used up to 70% when only ODA was used, confirming that the ether linkages in ODA lower the rigidity of the polyimide main chain. The flexible -O- linkages will stretch along the drawing direction, thereby consuming

part of the applied stress. Favored by the improved effect of the use of ODA on the mechanical properties of PI fibers (Fig.3), we found that PI/CA fibrous membranes obtained when only ODA was used in the synthesis of PAA (ODA: PDA 10:0) have a critical tensile stress and critical tensile strain of 130 MPa and 55%, respectively. Note that the use of ODA in the synthesis of PAA thus significantly increases the critical tensile strain of the thus obtained core/shell PI/CA membranes.

3.2. Morphological and thermal properties of core/shell structured PI/CA nanofibers/membranes synthesized with flexible PAA

In order to characterize the structure and morphology of the obtained nanofiber, TEM was applied. As shown in Fig. 5a, the PI/CA fibers showed a clear core/shell structure and the outer diameter of the fibers was approximately 200 nm with a wall thickness of approximately 5 nm, indicating that the PI nanofibers were coated by a thin CA layer; it looks very much like a high flexible PI wire (core) is inclusion into the CA fiber (shell). Therefore, the good mechanical performance of PI/CA nanofibers could be explained by the designed core/sheath structure (Fig. 4)[63, 64]

Subsequently, thermogravimetric analysis (TGA) curves of PI, CA and PI/CA fibrous membranes were shown in Fig. 5b. PI-based membrane presents a very stable status when heated before 530 ^{o}C (in nitrogen environment). However, CA-based membrane began to decompose when the temperature rises to 300 ^{o}C and decrease to about 15% of their mass upon further heating to 370 ^{o}C. Compared with CA- or PI-based membranes, PI/CA membrane shows two weight-loss processes due to the different heat resistances of the CA shell and PI core. The first pronounced weight loss about 35% from 300 to 370 ^{o}C is associated with the CA shell. The next step, in the range of about 530–620 °C, is due to the decomposition of the PI core. The results presented a further support for the above described structure of PI/CA nanofiber. Furthermore, the relatively high thermal stability of CA and core/shell structure PI/CA fibrous membranes below a temperature of 300 ^{o}C also verifies that the imidization of CA/PAA at 260 ^{o}C for 30 min did not damage the fibers, which is

advantageous for application in oil-water separation.

3.3. F-BZ coating of the flexible core/shell structured PI/CA nanofibers/membranes

In order to optimize the membrane design to achieve robust superhydrophobic and superoleophilic surface was effectively used for application in oil-water separation, the fibrous membrane was coated with fluorinated polybenzoxazine (F-PB) layer via in situ polymerization. The representative FE-SEM image of pristine CA, PI, and PI/CA nanofibers shown in Fig. 6a-c revealed a randomly oriented 3D nonwoven membrane with an average diameter of 2 μm for CA. In addition, the surface of uncoated CA fibrous membranes is relatively rough and many poles were appeared, while PI and PI/CA nanofibers display relatively smooth surface, especially for PI. Upon curing at 190 ^{o}C, the in situ polymerization of BAF-btfa monomers leads to the formation of the Mannich bridge cross-linked structure, and generating a cured thermosetting F-PB layer on the fiber surface. The morphology of the resulted F-PB modified electrospun fibrous membranes is presented in Fig. 6d-f, showing that adhesion has occurred with the addition of BAF-btfa. In addition, a cross-linked F-PB polymer thin layer was formed among the nanofibers voids such that the adjacent nanofibers could be cemented. This also indicated the BAF-btfa monomers was in situ polymerized on the surface of CA, PI, and PI/CA nanofibers successfully.

Evidence of the formation of F-PB modified surface of PI, CA and PI/CA nanofibers was also observed from FT-IR spectroscopy (Fig. S6). Fig. 7 shows the wetting property of water and oil on the surface of the membranes. As shown in Fig. 7a, the water contact angles (WCAs) increased gradually with increasing of BAF-btfa concentrations. The maximum value obtained was 112^{o} with 1 wt% of BAF-btfa added. In contrast, the oil contact angles (OCAs) were presented in Fig. 7b-d-f. After employing the F-PB modification, the pristine oleophilic fibrous membranes were endowed with a decreasing OCAs. Meanwhile, increasing the concentration of BAF-btfa at 1 wt% has decreased the OCAs values for PI, CA and PI/CA fibrous membranes to 2°, 5° and 1°, respectively, indicating the superoleophilicity of the modified membranes and could be ascribed to the BAF-btfa containing lipophilic benzene

that improves the oil wettability of the fibrous membranes. However, high concentration of BAF-btfa (> 1 wt%) could reduce the surface roughness of fibrous membranes leading to the lowered oleophilicity.

3.4. Modification of electrospun fibrous membranes by in situ polymerization in the presence of silica nanoparticles

Surface modification of the fibers with nanoparticles (e.g. SiO_2) to enhance the hydrophobicity of the surface has been reported[53, 65]. It is noteworthy mentioning that the properties of the BAF-btfa modified surfaces of the fibers have been further optimized by using BAF-btfa/n-butyl acetate solution with silica nanoparticles well dispersed to modify surfaces of the PI, CA and PI/CA fibrous membrane in order to be suitable for oil–water separation (see Scheme 1). As shown in Fig. 6g-h-i, by inclusion of SNPs in the F-PB layer, the morphology of the resulting membranes was remarkably changed by creating hierarchical structures containing numerous micro- and nano-scaled roughness on the surfaces of nanofibers. Moreover, the successful incorporation of SNPs in the membranes was also confirmed by FT-IR analysis (Fig. S6a(III) – c(III)).

To optimize the surface wettability of BAF-btfa and SNPs modified nanoporous membrane, orthogonal experiments were designed and conducted with different concentrations of BAF-btfa monomer and SNPs (Tab S1, Fig. 8). The results show that, with defined concentration of SNPs, a significant increase in membrane surface hydrophobicity. Moreover, the same trend is also observed for nanoparticle-free membranes (Fig. 8). In contrast to the influence of BAF-btfa concentration, the increase of SNPs results in a monotonous increase of both hydrophobicity (Fig. 8a-c-e) and oleophilicity (Fig. 8b-d-f), as their surface became rougher and rougher with the increasing SNPs content. Moreover, for CA-based and PI/CA-based fibrous membranes the highest WCA (around 163º) and a low OCA could be achieved by F-PB-1/SNP-4 modification. Compared with our previously published result[61], all of the modified fibrous membranes were showed much higher WCAs, which ascribed to

the addition of fluorine molecules to the polymer structure. Also note that the as-prepared PI/CA/F-PB-1/SNP-4/ fibrous membranes can maintain their superhydrophobicity after storing in air at room temperature for 7 months and the change in WCA of the membranes turned out to be less than 5% (Fig. S7).

Based on the above results, PI/CA/F-PB-1/SNP-4/ fibrous membranes, which show promising elongation behavior and which are super-hydrophobic were further evaluated for the oil-water separation purposes. Experimentally, dynamic contact angle was also measured by advancing/receding and sliding angle and sliding angle (the surface tilt angle that required for a droplet to move) to evaluate the hydrophobic performance. As shown in Fig. 9a, the advancing contact angle and receding contact angle of the as-prepared PI/CA/F-PB-1/SNP-4 membranes are 162.1^{o} and 155.7^{o}. Moreover, they exhibited slight contact angle hysteresis (the difference between the advancing and receding contact angles) of 6.3^{o}. It could be explained as follows, after BAF-btfa and SNPs modification, PI/CA membrane with higher water contact angle and thus more repellence was formed by air pockets. Then the water droplets could be pumped easily for the benefit of these air pockets between water and membrane surface. Furthermore, water droplet roll-off is investigated to support the low water adhesion of PI/CA/F-PB-1/SNP-4 membranes, where a sliding angle of ≈7.5° is obtained. Additionally, a high speed camera capture system was used to examine the adhesion and permeating process of a water droplets. As shown in Fig. 9b, when a water droplet touches and leaves the PI/CA/F-PB-1/SNP-4 membranes surface, almost no deformation occurred after it was lifted up to leave the membrane surface. Even the droplet was forced full contact with the membrane surface under the compression of an external force. In contrast, when the droplet of dichloromethane contacts the PI/CA/F-PB-1/SNP-4 membranes surface, it could quickly spread and permeated into the membranes within ≈ 150 ms. Based on the above results, PI/CA/F-PB-l/SNP-4fibrous membrane with excellent tensile stress and strain property, high super hydrophobicity as well as superoleophilicity were chosen for the oil-water separation application.

3.5. Evaluation of membrane in oil–water separation

To investigate the separation capability of PI/CA/F-PB-1/SNP-4 membranes, a solely gravity driven oil–water separation experiment was carried out. The experimental setup is schematically shown in Fig. 10d. it was flexible enough to be settled by fixing PI/CA/F-PB-1/SNP-4 membrane between two glass tube. A 20 mL mixture of oil dichloromethane (DCM) and water (50% v/v) was prepared and poured slowly onto the upper glass tube. Oil quickly permeated through the membranes and dropped into the beaker below. Meanwhile, water was retained above the membranes because of the superhydrophobicity and low water-adhesion properties of the membranes. No external force was employed during the fast separation process (within 3 min), only their own weight. In addition, the collected droplets did not form a liquid film across the surface of the membrane. And, they do not block the membrane, which can be seen from the results of Fig. 12c. Significantly, the total oil concentration in the collected water after separation (Fig. 10e) is less than 4 ppm even after ten times separation cycles.

The essence of oil-water separation is the wettability behavior of water and oil phase at the interface of the solid, air. surface free energy of a solid substrate plays a decisive role in the wettability. The wettability of a liquid droplet on a flat membrane is commonly determined by Young's equation[66]:

$$\cos\theta_0 = \frac{(\gamma_{SV} - \gamma_{SL})}{\gamma_{LV}} \qquad (7)$$

Where θ_0 is the CA in the Young's mode, γ_{SV} and γ_{LV} are the surface energies of the solid and vapor, liquid and vapor respectively, γ_{SL} is the interface tension between the solid and liquid. Since the surface tension for water and DCM are 72 and 23 mN · m^{-1}, respectively, therefore the oleophilic surface in air turn superhydrophobic in oil. The PI/CA/F-PB-1/SNP-4 became superhydrophobic when under the oil. The rough surface structure and superhydrophobicity of the PI/CA/F-PB-1/SNP-4 resulting a particular wettability characterizing a water/oil/solid three-phase system. When the PI/CA/F-PB-1/SNP-4

membranes were immersed in oil, oil became trapped within its rough microstructure that then formed a water/oil/solid interface. The contact area between the water droplet and the surface of the PI/CA/F-PB-1/SNP-4 was decreased significantly due to the trapped oil molecules, thus leading to superhydrophobicity. While air is trapped under the droplet in surface cavities forming a composite solid–water–air wetting state, the apparent CA (θ_C) could be described as Cassie equation[67]:

$$\cos\theta_C = f_s \cos\theta_0 + f_s - 1. \qquad (8)$$

Where, f_s is the area fraction on the surface. Therefore, when f_s decreases for a larger roughness surface, the WCA increases. The PI/CA/F-PB-1/SNP-4 fibrous membrane possess a very rough surface, which indicate a relative small area fraction, thus a large water contact angle.

To make clear of the oil-water separation process, the water and oil wetting processes are modeled in Fig. 11. Generally, the liquid can wet the pore bottom only after an intrusion pressure ΔP has to be overcome because the advancing contact angle θ_A has to be exceeded, which can be described as follows[68, 69]

$$\Delta P = -\frac{2\gamma}{R} = -\frac{\iota\lambda\cos\theta_A}{A} \qquad (9)$$

where γ is the surface tension, R is the meniscus's radius, ι is the pore's perimeter, θ_A is the advancing contact angle on the membrane, and A is the pore's area. As can be seen from equation 9, when θ_A > 90°, the membrane can withstand the pressure to some extent since the $\Delta P > 0$. In this work, the membrane displays superhydrophobicity and superoleophilicity, for water contact angle the θ_A is apparently larger than 90°; therefore, the water cannot pass the membrane (Fig. 11c and Fig. 11a), As to oil contact angle, the membrane displays superoleophilicity, and θ_A is nearly 0°. Based on the above proposed equation, $\Delta P < 0$, reveling the oil can pass through the membrane and the process occur spontaneously because

the membrane cannot support any pressure (Fig. 11c). After the permeation process, the interspaces between the SNPs and PI nanofiber would be occupied by oil for the superoleophilicity of the membrane. The trapping of oil can enhance the water-repellent force, which can lead to the superhydrophobicity and high WCA on the membrane (Fig. 11b, the WCA is larger than 90°). Thus, the water cannot pass through the membrane as the $\Delta P > 0$ (Fig. 11c). From the discussed above, it is clear that the membrane has a good superhydrophobicity and superoleophilicity and an oil-water mixture can be well separated with the membrane.

Subsequently, the results of oil flux test for electrospun fibrous membranes were shown in Fig. 12a-b. The flux of DCM through the flexible PI/CA membranes is significantly high, which indicates that the core/shell PI/CA fibrous membranes have much attractive properties after surface modification. Moreover, with the increasing of the content of BAF-btfa and SNPs, the flux through the modified CA–PI fibrous membranes were found to be improved. This could be attributed to the higher WCAs and the lower OCAs, which have also been proposed by others[70]. Moreover, the filtrate flux of DCM-water through PI/CA/F-PB-1/SNP-4 membrane even equaled 3106 ± 100 L m^{-2} h^{-1}, which is significantly 15 times higher than the fluxes through commercial filtration membranes (20-200 $L \cdot m^{-2} \cdot h^{-1}$[35]). The pore size and pore size distribution of the fibrous membranes (Fig. S8) could be used as an explanation for this. However, for CA membrane, it could not separate through newly developed separation device even though it possesses the properties of superhydrophobicity and superoleophilicity, which could be ascribed to poor tensile stress of CA membrane. When oil-water mixture poured slowly onto the upper glass tube, the CA membranes were broken (Fig. S9.)

In addition, the different the antifouling performance presented in Fig. 12c show minimal flux fluctuation after ten separation cycles, which indicates the excellent reusability of the designed fibrous membranes. Besides DCM-water mixture, a variety of organic solvent/water mixtures including trichloromethane-water, carbon tetrachloride-water, dichloromethane-water and bromobenzene-water have been successfully separated through

the same process (Fig. 12d).

The results in Fig. 12e-f shows the separation efficiency of the membranes for DCM-water mixtures, as has been defined by equation 2. Clearly, the core/shell structure PI/CA fibrous membranes have a high separation efficiency (> 99.5%) and the oil (DCM) permeability through the membrane was 87.82% (Tab. S2), regardless of the concentrations for BAF-btfa and SNPs. Moreover, the electrospun PI/CA fibrous membranes shows high and stable separation efficiency (>98%, see Fig. 12g) even after ten times separation cycles, Significantly, the PI/CA fibrous membranes exhibit extremely high separation efficiency for different kinds of oil-water mixtures (Fig. 12h).

To further study the separation performance of the PI/CA/F-PB-1/SNP-4 membranes, the intrusion pressure of the water flowing through the membrane was measured. Which indicate the maximum weight of the water of PI/CA/F-PB-1/SNP-4 membranes can support. The intrusion pressure is provided by the weight of water, which is calculated using equation (6). Results show the intrusion pressures for water in our system was about 9.31 kPa. It means that water cannot flow through the membrane below the intrusion. In addition, Fluxes of 10 mL DCM through PI/CA/F-PB-1/SNP-4 fibrous membranes with different height of glass tubes filled with oil and water (Fig. 13) were used to character higher flux results from higher pressure.

For PI/CA/F-PB-l/SNP-4 membranes, the DCM-flux and separation efficiency as a function of the membrane thickness was also tested (Fig. 14a-b). As shown in Fig. 14c, the thinner membranes yield higher porosity, which benefits the formation of channel for oil to through, resulting the increased permeation flux through the thinner membranes (Fig. 14a). Meanwhile, the separation efficiency was not significantly influenced by the membrane thickness (Fig. 14b) indicating the possibility to optimize the membrane thickness to obtain separation device with high flux. Furthermore, four different proportions mixtures of DCM-water were also tested for separation (Fig. S10), demonstrating all of these samples were well separated independent of the different proportions of oil-water mixtures and the higher proportions of

water in the mixture led to higher flux due to the higher hydraulic pressure.

Chemical stability test was performed to evaluate the effect of pH to the PI/CA/F-PB-l/SNP-4 membrane's wettability. As seen in Fig. 15a, the WCAs was maintained at an ultrahigh value of about 160^{o} towards abroad range of pH (1−13), suggesting its excellent stability against extreme pH condition. This implies that the membrane is superior over those commercial membranes. The hybrid membrane's hydrophobicity after calcination for 10min at various temperatures (100-450 °C, ramping rate of 10 °C/min) was also investigated. As shown in Fig. 15b, the hydrophobicity is maintained after annealing treatment up to 400 °C. At 450 °C, the membrane lost its constancy of hydrophobicity which can be manifested by the substantial drop in WCA close to 18°, this may be attributed to the decomposition of CA nanofibers. In addition, when heated the PI/CA membranes in air at different temperature (Fig. 15c) the as-prepared fibrous membranes can maintain its hydrophobicity until 180°C. Several inferences can be drawn from the above results. Firstly, the membrane wetting properties is switchable between hydrophobic and hydrophilic states by modifying the surface with hydrophobic/hydrophilic materials that can be removed at elevated calcination temperature. Secondly, with stable hydrophobicity at high temperature (400 °C), the membrane should be able to serve effectively separation under high temperature condition such as oil spill incidents accompanied by a great fire due to burning of oil spill. Thirdly, the oil-fouled membrane can be easily regenerated and reused by means of calcination and chemical cleaning. Therefore, these PI/CA/F-PB-1/SNP-4 membranes are good candidates for industrial oil-polluted water treatments and oil spill clean-up.

4. Conclusions

In summary, free-standing, high flexible fibrous membranes, with a superhydrophobic and superoleophilic surface wettability, were fabricated by the combination of electrospun core-sheath structured PI/CA nanofibers and a novel in-situ polymerized F-PB functional containing SNPs. The core/shell structure PI/CA nanofibers inherit both the high mechanical property of a PI fiber core and the surface roughness of a CA shell. After surface modification

with F-PB/SNPs, the membranes become superhydrophobic and superoleophilic. The ether linkage in polyamide acid and the additional fluorine molecules of BAF-btfa clearly improved the deformation properties and the hydrophobicity of the fibers. We anticipate that this work will provide a versatile avenue for the fabrication of membranes which are excellently suited for an energy-efficient separation of various oil-water mixtures.

Acknowledgements

Jiangsu key lab of biomass-based energy and Materials (JSBEM2016011), National Natural Science Foundation of China (No.21644004), Jiangsu specially-appointed professorship program (Sujiaoshi [2012]34) , Priority Academic Program Development of Jiangsu Higher Education Institutions (PAPD), Top-notch Academic Programs Project of Jiangsu Higher Education Institutions (TAPP), Scientific Research Staring Foundation for the Returned Overseas Chinese Scholars, Ministry of Education of China and Jiangsu key lab of biomass-based green fuels and chemicals (JSBGFC14001) and Natural Science Key Project of the Jiangsu Higher Education Institutions (16KJA220006) are acknowledged with gratitude. We also thank Advanced Analysis & Testing Center, Nanjing Forestry University for SEM characterization.

References

[1] X. Feng, L. Jiang, Design and creation of superwetting/antiwetting surfaces, Advanced Materials, 18 (2006) 3063-3078.

[2] K. Liu, X. Yao, L. Jiang, Recent developments in bio-inspired special wettability, Chemical Society Reviews, 39 (2010) 3240-3255.

[3] Z. Xue, S. Wang, L. Lin, L. Chen, M. Liu, L. Feng, L. Jiang, A novel superhydrophilic and underwater superoleophobic hydrogel‐coated mesh for oil/water separation, Advanced Materials, 23 (2011) 4270-4273.

[4] B. Wang, Z. Guo, pH-responsive bidirectional oil–water separation material, Chemical Communications, 49 (2013) 9416-9418.

[5] J. Zhang, S. Seeger, Polyester materials with superwetting silicone nanofilaments for oil/water separation and selective oil absorption, Advanced Functional Materials, 21 (2011) 4699-4704.

[6] S.-J. Choi, T.-H. Kwon, H. Im, D.-I. Moon, D.J. Baek, M.-L. Seol, J.P. Duarte, Y.-K. Choi, A polydimethylsiloxane (PDMS) sponge for the selective absorption of oil from water, ACS applied materials & interfaces, 3 (2011) 4552-4556.

[7] A.K. Kota, G. Kwon, W. Choi, J.M. Mabry, A. Tuteja, Hygro-responsive membranes for effective oil–water separation, Nature communications, 3 (2012) 1025.

[8] Y. Wang, S. Tao, Y. An, A reverse membrane emulsification process based on a hierarchically

porous monolith for high efficiency water–oil separation, Journal of Materials Chemistry A, 1 (2013) 1701-1708.
[9] X. Tang, Y. Si, J. Ge, B. Ding, L. Liu, G. Zheng, W. Luo, J. Yu, In situ polymerized superhydrophobic and superoleophilic fibrous membranes for gravity driven oil–water separation, Nanoscale, 5 (2013) 11657-11664.
[10] M.H. Tai, P. Gao, B.Y.L. Tan, D.D. Sun, J.O. Leckie, Highly Efficient and Flexible Electrospun Carbon–Silica Nanofibrous Membrane for Ultrafast Gravity-Driven Oil–Water Separation, ACS applied materials & interfaces, 6 (2014) 9393-9401.
[11] V.K. Gupta, A. Rastogi, A. Nayak, Adsorption studies on the removal of hexavalent chromium from aqueous solution using a low cost fertilizer industry waste material, Journal of Colloid and Interface Science, 342 (2010) 135-141.
[12] Q. Huang, F. Mao, X. Han, J. Yan, Y. Chi, Migration of Emulsified Water Droplets in Petroleum Sludge during Centrifugation, Energy & Fuels, 28 (2014) 4918-4924.
[13] M. Yeber, E. Paul, C. Soto, Chemical and biological treatments to clean oily wastewater: optimization of the photocatalytic process using experimental design, Desalination and Water Treatment, 47 (2012) 295-299.
[14] X. Xu, X. Zhu, Treatment of refectory oily wastewater by electro-coagulation process, Chemosphere, 56 (2004) 889-894.
[15] Q. Wen, J. Di, L. Jiang, J. Yu, R. Xu, Zeolite-coated mesh film for efficient oil–water separation, Chemical Science, 4 (2013) 591-595.
[16] J. Lahann, Environmental nanotechnology: Nanomaterials clean up, Nature nanotechnology, 3 (2008) 320-321.
[17] X. Yao, Y. Song, L. Jiang, Applications of Bio‐Inspired Special Wettable Surfaces, Advanced Materials, 23 (2011) 719-734.
[18] W. Ma, Q. Zhang, S.K. Samal, F. Wang, B. Gao, H. Pan, H.-J. Xu, J. Yao, X. Zhan, S. De Smedt, Core-sheath Structured Electrospun Nanofibrous Membranes for Oil-water Separation, RSC Advances, (2016).
[19] N. Bhardwaj, S.C. Kundu, Electrospinning: a fascinating fiber fabrication technique, Biotechnology advances, 28 (2010) 325-347.
[20] A. Greiner, J.H. Wendorff, Electrospinning: a fascinating method for the preparation of ultrathin fibers, Angewandte Chemie International Edition, 46 (2007) 5670-5703.
[21] L. Zhang, X. Gong, Y. Bao, Y. Zhao, M. Xi, C. Jiang, H. Fong, Electrospun nanofibrous membranes surface-decorated with silver nanoparticles as flexible and active/sensitive substrates for surface-enhanced Raman scattering, Langmuir, 28 (2012) 14433-14440.
[22] C. Huang, S.J. Soenen, J. Rejman, B. Lucas, K. Braeckmans, J. Demeester, S.C. De Smedt, Stimuli-responsive electrospun fibers and their applications, Chemical Society Reviews, 40 (2011) 2417-2434.
[23] S.A.A.N. Nasreen, S. Sundarrajan, S.A.S. Nizar, R. Balamurugan, S. Ramakrishna, Advancement in electrospun nanofibrous membranes modification and their application in water treatment, Membranes, 3 (2013) 266-284.
[24] W. Ma, Q. Zhang, D. Hua, R. Xiong, J. Zhao, W. Rao, S. Huang, X. Zhan, F. Chen, C. Huang, Electrospun fibers for oil–water separation, RSC Advances, 6 (2016) 12868-12884.
[25] H.-r. Nie, C. Wang, Fabrication and chemical crosslinking of electrospun trans-polyisoprene nanofiber nonwoven, Chinese Journal of Polymer Science, 34 (2016) 697-708.

[26] Z.-y. Fan, Y.-l. Zhao, Y. Luo, M.-w. Shen, Folic acid modified electrospun poly (vinyl alcohol)/polyethyleneimine nanofibers for cancer cell capture applications, Chinese Journal of Polymer Science, 34 (2016) 755-765.
[27] S. Jian, X.w. Hu, Y. Zou, S. Chen, H. Hou, The preparation of characterization for high-strength electrospun polyimide/Ag composite nanofibres, Journal of Jiangxi normal university(Naturnal science), 36 (2012) 1-4.
[28] M.W. Lee, S. An, S.S. Latthe, C. Lee, S. Hong, S.S. Yoon, Electrospun polystyrene nanofiber membrane with superhydrophobicity and superoleophilicity for selective separation of water and low viscous oil, ACS applied materials & interfaces, 5 (2013) 10597-10604.
[29] X. Wang, D. Fang, K. Yoon, B.S. Hsiao, B. Chu, High performance ultrafiltration composite membranes based on poly (vinyl alcohol) hydrogel coating on crosslinked nanofibrous poly (vinyl alcohol) scaffold, Journal of Membrane Science, 278 (2006) 261-268.
[30] Z. Tang, J. Wei, L. Yung, B. Ji, H. Ma, C. Qiu, K. Yoon, F. Wan, D. Fang, B.S. Hsiao, UV-cured poly (vinyl alcohol) ultrafiltration nanofibrous membrane based on electrospun nanofiber scaffolds, Journal of Membrane Science, 328 (2009) 1-5.
[31] J. Kong, K. Li, Oil removal from oil-in-water emulsions using PVDF membranes, Separation and purification technology, 16 (1999) 83-93.
[32] Z. Zhao, J. Zheng, M. Wang, H. Zhang, C.C. Han, High performance ultrafiltration membrane based on modified chitosan coating and electrospun nanofibrous PVDF scaffolds, Journal of membrane science, 394 (2012) 209-217.
[33] M. Sivakumar, A. Mohanasundaram, D. Mohan, K. Balu, R. Rangarajan, Modification of cellulose acetate: Its characterization and application as an ultrafiltration membrane, Journal of applied polymer science, 67 (1998) 1939-1946.
[34] L. Yang, A. Thongsukmak, K.K. Sirkar, K.B. Gross, G. Mordukhovich, Bio-inspired onboard membrane separation of water from engine oil, Journal of Membrane Science, 378 (2011) 138-148.
[35] B. Chakrabarty, A. Ghoshal, M. Purkait, Ultrafiltration of stable oil-in-water emulsion by polysulfone membrane, Journal of Membrane Science, 325 (2008) 427-437.
[36] R.W. Baker, Membrane technology, Wiley Online Library, 2000.
[37] Y. Teow, A. Ahmad, J. Lim, B. Ooi, Preparation and characterization of PVDF/TiO 2 mixed matrix membrane via in situ colloidal precipitation method, Desalination, 295 (2012) 61-69.
[38] S.B. Teli, S. Molina, A. Sotto, E.G.a. Calvo, J.d. Abajob, Fouling resistant polysulfone–PANI/TiO2 ultrafiltration nanocomposite membranes, Industrial & Engineering Chemistry Research, 52 (2013) 9470-9479.
[39] S. Yu, X. Zuo, R. Bao, X. Xu, J. Wang, J. Xu, Effect of SiO 2 nanoparticle addition on the characteristics of a new organic–inorganic hybrid membrane, Polymer, 50 (2009) 553-559.
[40] M. Khayet, J. Villaluenga, J. Valentin, M. López-Manchado, J. Mengual, B. Seoane, Filled poly (2, 6-dimethyl-1, 4-phenylene oxide) dense membranes by silica and silane modified silica nanoparticles: characterization and application in pervaporation, Polymer, 46 (2005) 9881-9891.
[41] L. Jin, S. Yu, W. Shi, X. Yi, N. Sun, Y. Ge, C. Ma, Synthesis of a novel composite nanofiltration membrane incorporated SiO 2 nanoparticles for oily wastewater desalination, Polymer, 53 (2012) 5295-5303.
[42] M. Obaid, N.A. Barakat, O. Fadali, M. Motlak, A.A. Almajid, K.A. Khalil, Effective and reusable oil/water separation membranes based on modified polysulfone electrospun nanofiber mats, Chemical Engineering Journal, 259 (2015) 449-456.

[43] G. Arthanareeswaran, T.S. Devi, M. Raajenthiren, Effect of silica particles on cellulose acetate blend ultrafiltration membranes: Part I, Separation and Purification Technology, 64 (2008) 38-47.
[44] F. Liu, B.-R. Ma, D. Zhou, Y.-h. Xiang, L.-x. Xue, Breaking through tradeoff of Polysulfone ultrafiltration membranes by zeolite 4A, Microporous and mesoporous materials, 186 (2014) 113-120.
[45] Y. Medina-Gonzalez, J.-C. Remigy, Sonication-assisted preparation of pristine MWCNT–polysulfone conductive microporous membranes, Materials Letters, 65 (2011) 229-232.
[46] Y. Zhang, L. Wang, Y. Xu, ZrO 2 solid superacid porous shell/void/TiO 2 core particles (ZVT)/polyvinylidene fluoride (PVDF) composite membranes with anti-fouling performance for sewage treatment, Chemical Engineering Journal, 260 (2015) 258-268.
[47] G. Arthanareeswaran, P. Thanikaivelan, Fabrication of cellulose acetate–zirconia hybrid membranes for ultrafiltration applications: performance, structure and fouling analysis, Separation and Purification Technology, 74 (2010) 230-235.
[48] A. Bottino, G. Capannelli, A. Comite, Preparation and characterization of novel porous PVDF-ZrO 2 composite membranes, Desalination, 146 (2002) 35-40.
[49] X. Zhang, Y. Wang, Y. Liu, J. Xu, Y. Han, X. Xu, Preparation, performances of PVDF/ZnO hybrid membranes and their applications in the removal of copper ions, Applied Surface Science, 316 (2014) 333-340.
[50] J. Hong, Y. He, Effects of nano sized zinc oxide on the performance of PVDF microfiltration membranes, Desalination, 302 (2012) 71-79.
[51] P. Gunawan, C. Guan, X. Song, Q. Zhang, S.S.J. Leong, C. Tang, Y. Chen, M.B. Chan-Park, M.W. Chang, K. Wang, Hollow fiber membrane decorated with Ag/MWNTs: toward effective water disinfection and biofouling control, ACS nano, 5 (2011) 10033-10040.
[52] Y. Shang, Y. Si, A. Raza, L. Yang, X. Mao, B. Ding, J. Yu, An in situ polymerization approach for the synthesis of superhydrophobic and superoleophilic nanofibrous membranes for oil–water separation, Nanoscale, 4 (2012) 7847-7854.
[53] J. Huang, S. Li, M. Ge, L. Wang, T. Xing, G. Chen, X. Liu, S. Al-Deyab, K.-Q. Zhang, T. Chen, Robust superhydrophobic TiO 2@ fabrics for UV shielding, self-cleaning and oil–water separation, Journal of Materials Chemistry A, 3 (2015) 2825-2832.
[54] Y. Wang, C. Lai, H. Hu, Y. Liu, B. Fei, J.H. Xin, Temperature-responsive nanofibers for controllable oil/water separation, RSC Advances, 5 (2015) 51078-51085.
[55] S. Tamai, A. Yamaguchi, M. Ohta, Melt processible polyimides and their chemical structures, Polymer, 37 (1996) 3683-3692.
[56] G. Eastmond, J. Paprotny, Scope in the synthesis and properties of poly (ether imide) s, Reactive and Functional Polymers, 30 (1996) 27-41.
[57] G. Eastmond, M. Gibas, J. Paprotny, Pendant adamantyl poly (ether imide) s: synthesis and a preliminary study of properties, European polymer journal, 35 (1999) 2097-2106.
[58] F. Li, S. Fang, J.J. Ge, P.S. Honigfort, J.-C. Chen, F.W. Harris, S.Z. Cheng, Diamine architecture effects on glass transitions, relaxation processes and other material properties in organo-soluble aromatic polyimide films, Polymer, 40 (1999) 4571-4583.
[59] M. Hasegawa, N. Sensui, Y. Shindo, R. Yokota, Structure and properties of novel asymmetric biphenyl type polyimides. Homo-and copolymers and blends, Macromolecules, 32 (1999) 387-396.
[60] S. Pyo, S. Kim, T. Shin, Y. Park, M. Ree, Synthesis and characterization of fully rodlike poly (4, 4′-biphenylene pyromellitimide) s with various short side groups, Journal of Polymer Science Part A: Polymer Chemistry, 37 (1999) 937-957.

[61] W. Ma, Q. Zhang, S.K. Samal, F. Wang, B. Gao, H. Pan, H. Xu, J. Yao, X. Zhan, S.C. De Smedt, Core–sheath structured electrospun nanofibrous membranes for oil–water separation, RSC Advances, 6 (2016) 41861-41870.
[62] L. Liu, S. Jiang, Y. Sun, S. Agarwal, Giving Direction to Motion and Surface with Ultra ‐ Fast Speed Using Oriented Hydrogel Fibers, Advanced Functional Materials, (2015).
[63] S. Rana, J.W. Cho, Core-sheath polyurethane-carbon nanotube nanofibers prepared by electrospinning, Fibers and Polymers, 12 (2011) 721-726.
[64] F. Kayaci, C. Ozgit-Akgun, I. Donmez, N. Biyikli, T. Uyar, Polymer–inorganic core–shell nanofibers by electrospinning and atomic layer deposition: Flexible nylon–ZnO core–shell nanofiber mats and their photocatalytic activity, ACS applied materials & interfaces, 4 (2012) 6185-6194.
[65] M. Huang, Y. Si, X. Tang, Z. Zhu, B. Ding, L. Liu, G. Zheng, W. Luo, J. Yu, Gravity driven separation of emulsified oil–water mixtures utilizing in situ polymerized superhydrophobic and superoleophilic nanofibrous membranes, Journal of Materials Chemistry A, 1 (2013) 14071-14074.
[66] T. Onda, S. Shibuichi, N. Satoh, K. Tsujii, Super-water-repellent fractal surfaces, Langmuir, 12 (1996) 2125-2127.
[67] J. Drelich, J.D. Miller, A. Kumar, G.M. Whitesides, Wetting characteristics of liquid drops at heterogeneous surfaces, Colloids and Surfaces A: Physicochemical and Engineering Aspects, 93 (1994) 1-13.
[68] J.P. Youngblood, T.J. McCarthy, Ultrahydrophobic polymer surfaces prepared by simultaneous ablation of polypropylene and sputtering of poly (tetrafluoroethylene) using radio frequency plasma, Macromolecules, 32 (1999) 6800-6806.
[69] B. Liu, F.F. Lange, Pressure induced transition between superhydrophobic states: configuration diagrams and effect of surface feature size, Journal of colloid and interface science, 298 (2006) 899-909.
[70] A. Al-Amoudi, P. Williams, A. Al-Hobaib, R.W. Lovitt, Cleaning results of new and fouled nanofiltration membrane characterized by contact angle, updated DSPM, flux and salts rejection, Applied Surface Science, 254 (2008) 3983-3992.

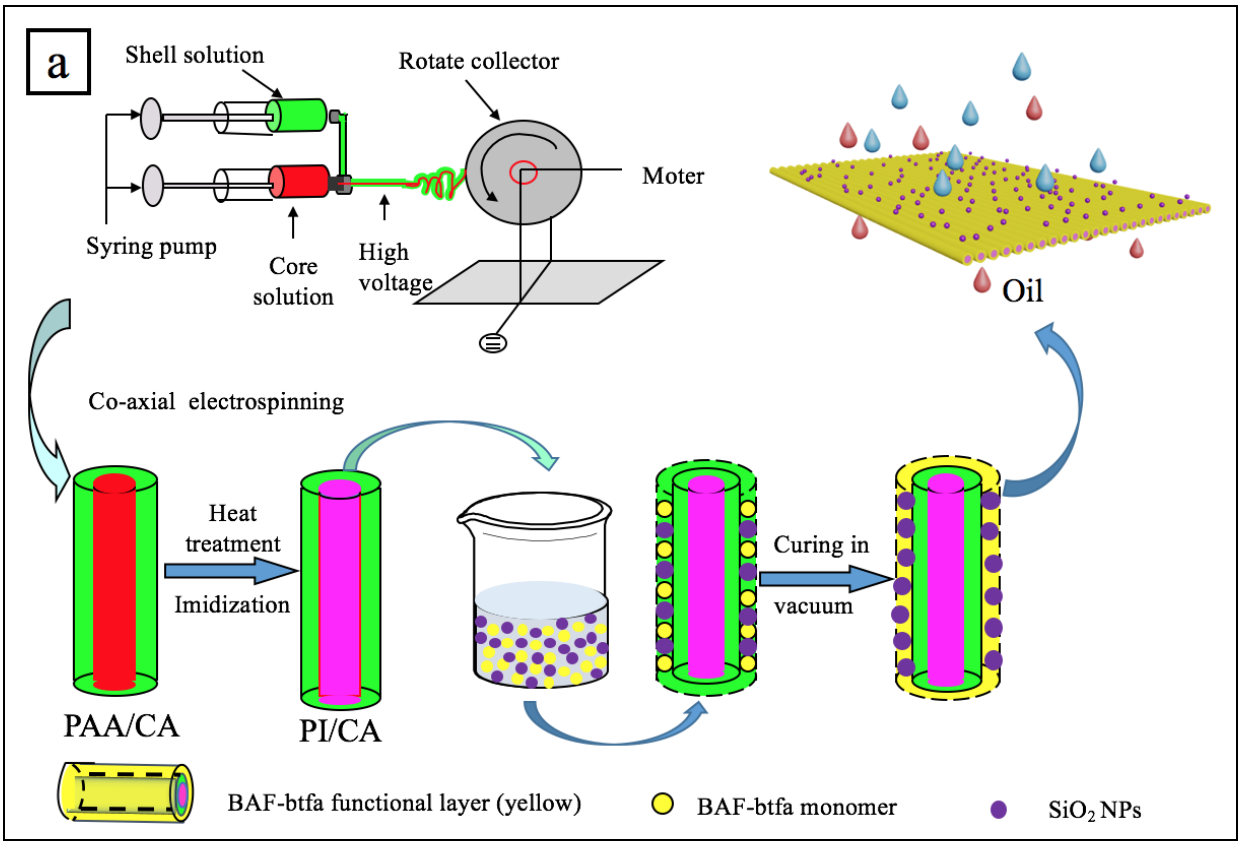
a
Shell solution
Rotate collector
Moter
Syring pump
Core solution
High voltage
Oil
Co-axial electrospinning
Heat treatment
Imidization
Curing in vacuum
PAA/CA
PI/CA
BAF-btfa functional layer (yellow)
BAF-btfa monomer
SiO2 NPs

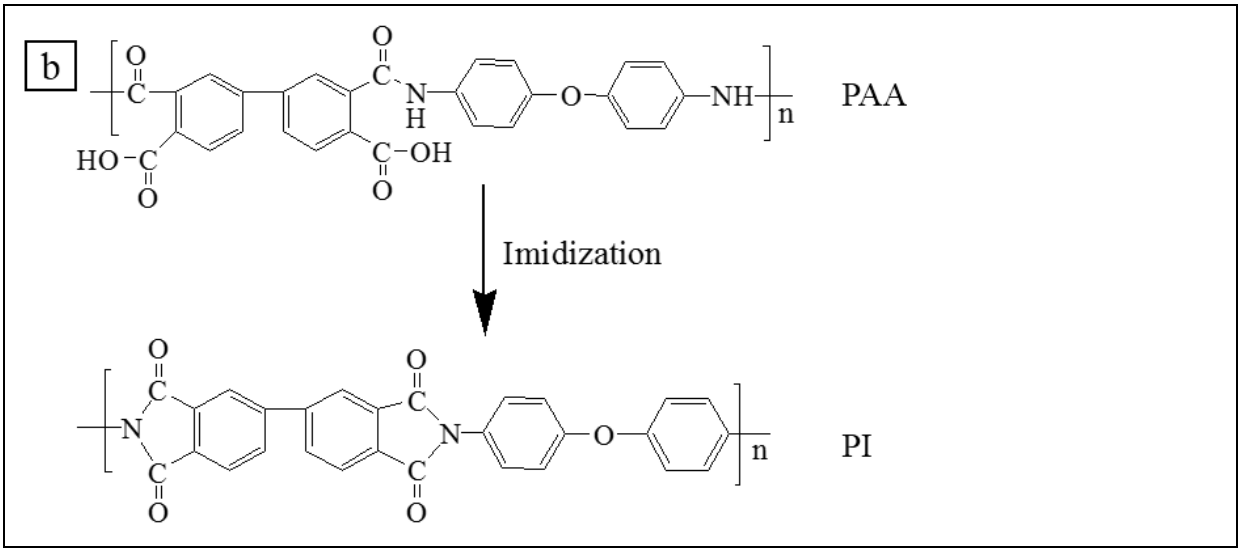

Scheme 1 (a) F-PB/SNP modified PI/CA nanofibrous membranes prepared through co-axial electrospinning: cellulose-acetate (CA-shell), polyamide acid (PAA-core), polyimide (PI-core); (b) Shows the imidization of PAA.

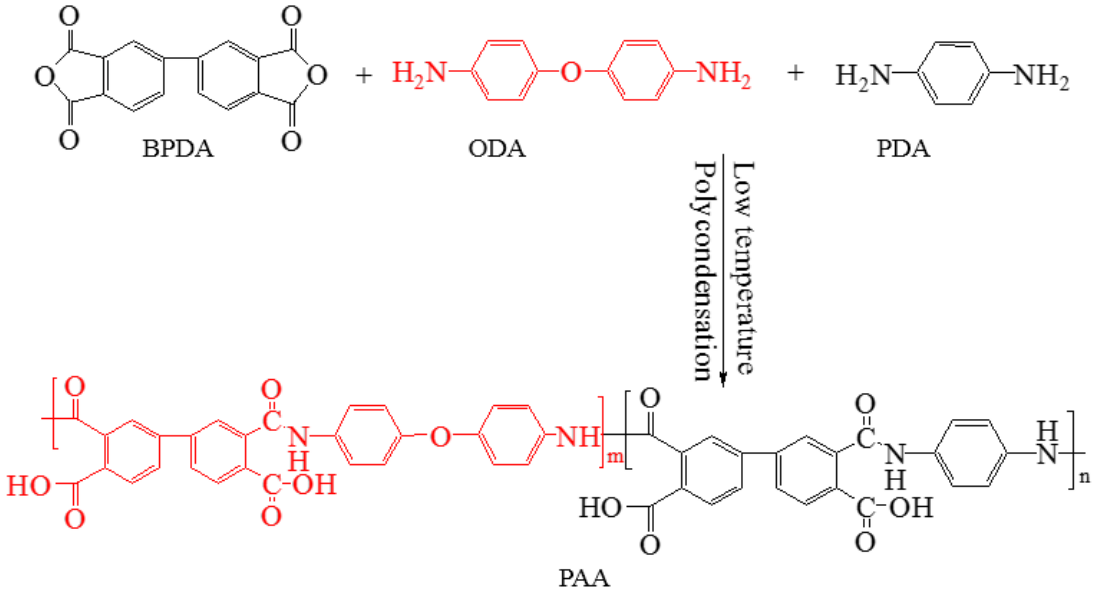

Fig. 1. Synthesis of 'flexible' polyamide acid (with ether linkages in the backbone); While in our previous study only p-phenylenediamine (PDA) was used, in the present study mixtures of 4,4'-diaminodiphenyl ether (ODA) and PDA were used in the synthesis of the PAA.

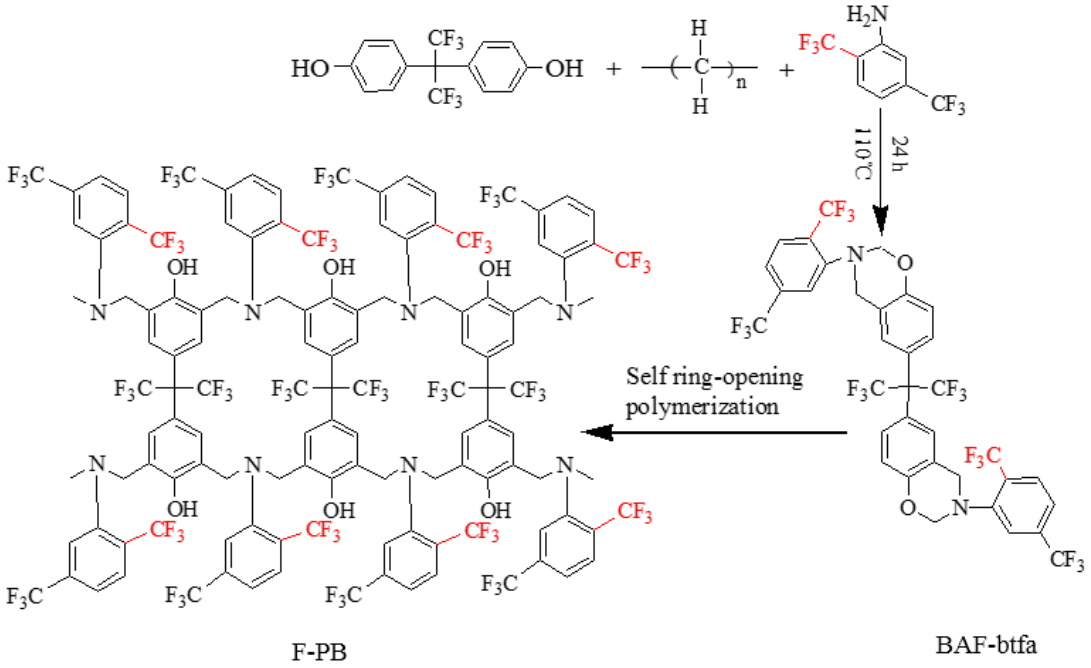

Fig. 2. Synthesis of 'heavily' fluorinated benzoxazine (BAF-btfa) and subsequent polymerization**.**

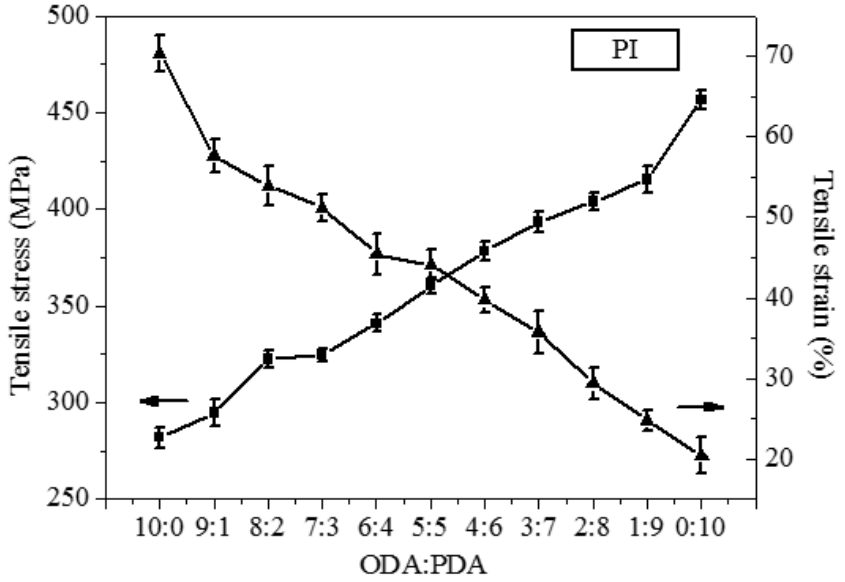

Fig. 3 (Critical) stress and strain of PI membranes obtained from PAA synthesized with ODA/PDA mixtures varying in molar ratio. Each type of membrane was three times synthesized; the critical stress and strain of each membrane was ten times measured.

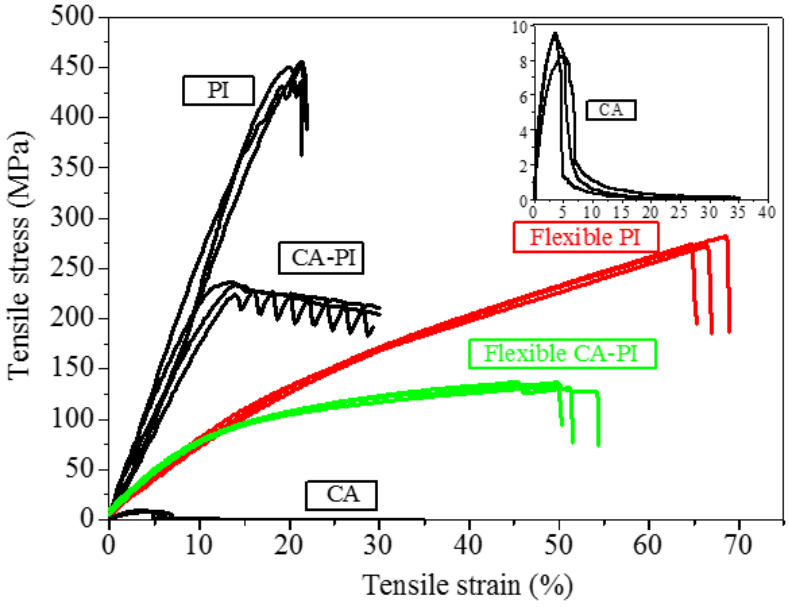

Fig. 4 Stress-strain curves (elongation behavior) of CA (insert), PI and core/shell PI/CA membranes. An ODA/PDA molar ratio of 0:10 was used for the PI and the PI/CA membranes. An ODA/PDA molar ratio of 10:0 was used for the 'flexible PI' and the 'flexible PI/CA' membranes.

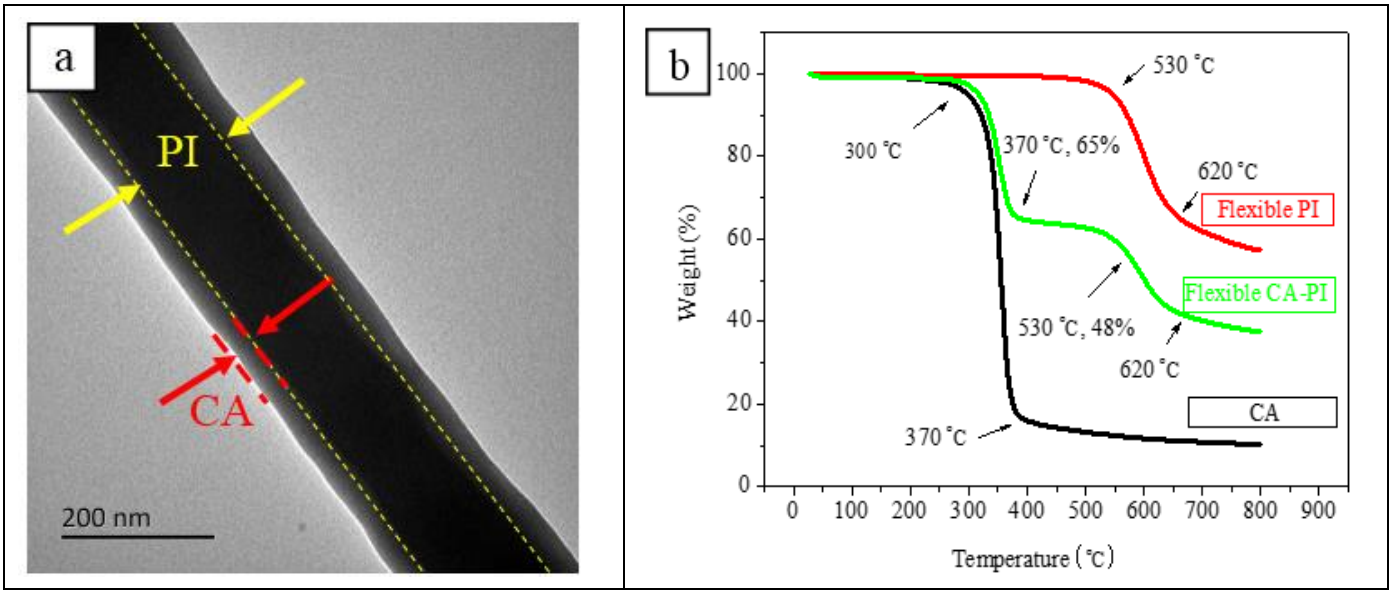

Fig. 5 (a) TEM image of a (flexible) PI/CA nanofiber (ODA/PDA molar ratio of 10:0); (b) TGA curves obtained on CA, flexible PI, and flexible PI/CA nanofibrous membranes (an ODA/PDA molar ratio of 10:0 was used for the PI and PI/CA membranes).

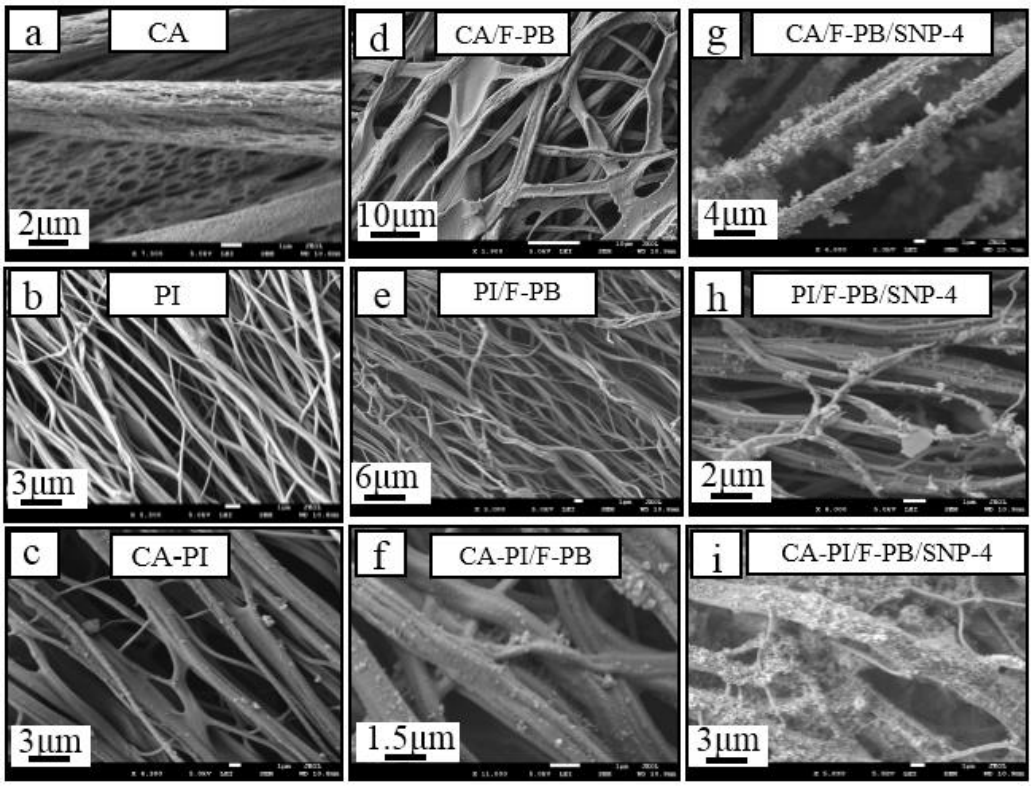

Fig. 6 FE-SEM images of electrospun fibrous membranes. For the PI and PI/CA membranes an ODA/PDA molar ratio of 10:0 was used.

Water contact angles (WCAs)	Oil contact angles (WCAs)

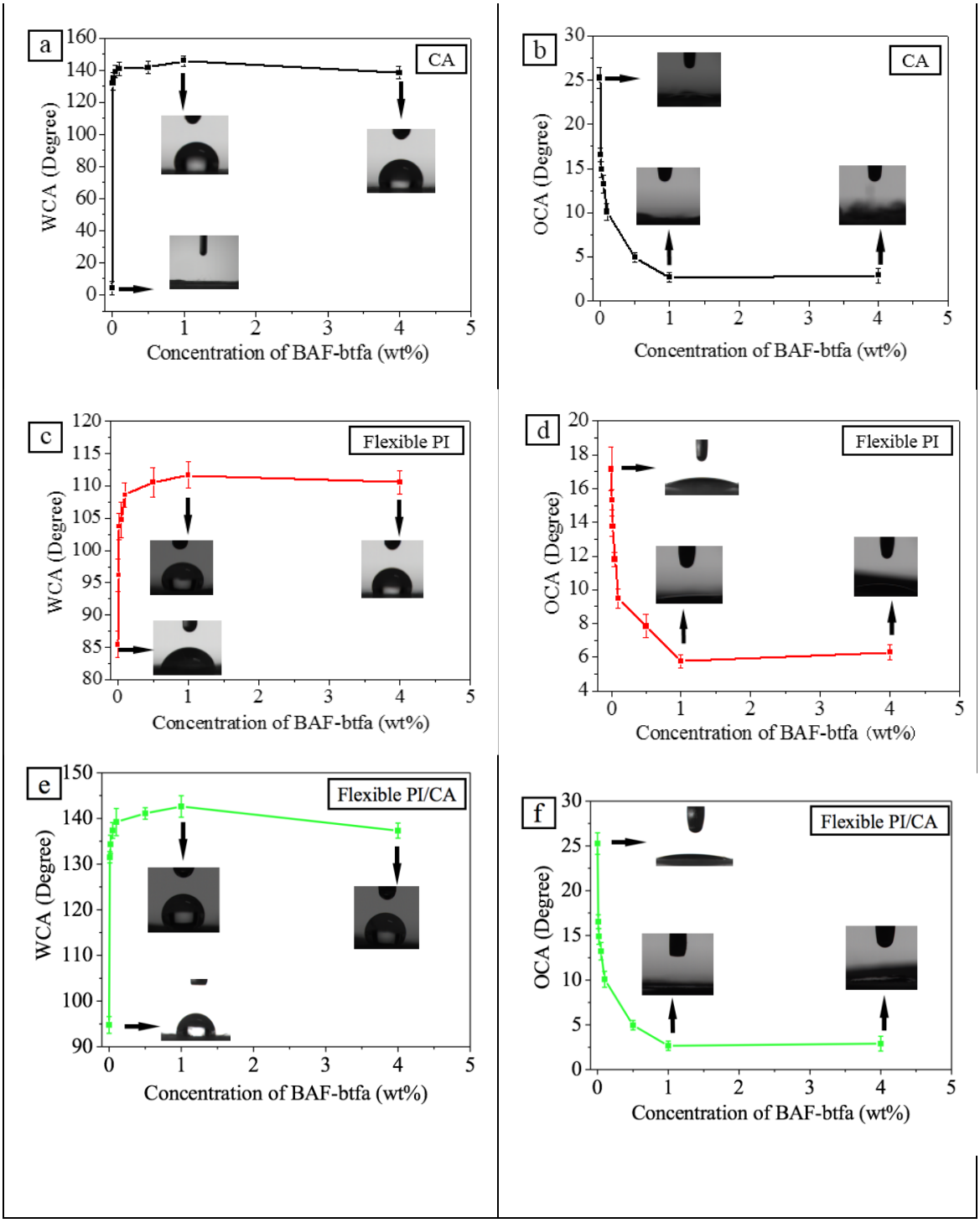

Fig. 7 WCAs (a, c, e) and OCAs (b, d, f) of CA, flexible PI and flexible core/shell PI/CA membranes modified with different concentrations of BAF-btfa. For the PI and PI/CA membranes an ODA/PDA molar ratio of 10:0 was used. All the contact angles were measured five times (n = 5).

Water contact angles (WCAs)	Oil contact angles (WCAs)

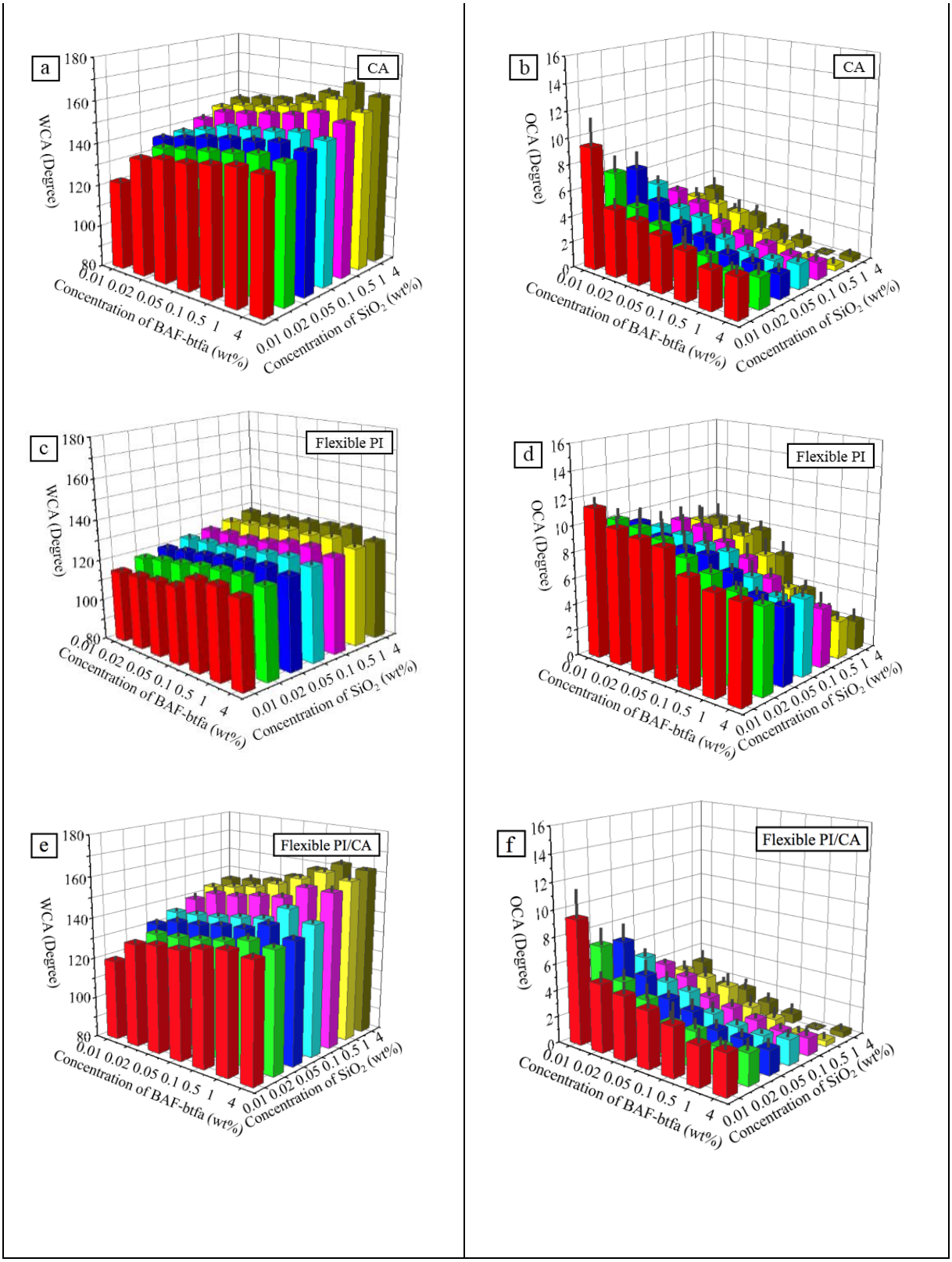

Fig. 8 WCAs (left) and OCAs (right) of CA (a, b), flexible PI (c, d) and flexible PI/CA (e, f) membranes modified with different concentrations of BAF-btfa and SNPs. For the PI and PI/CA membranes an ODA/PDA molar ratio of 10:0 was used. All the contact angles were measured five times (n = 5).

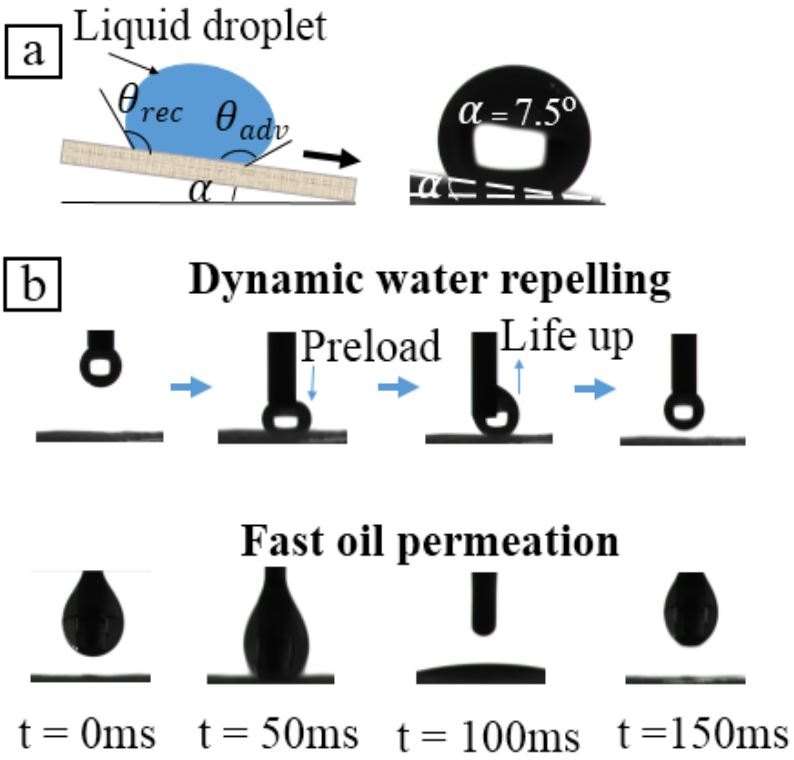

Fig. 9 a) left: schematic illustration of the sliding, advancing and receding angle of a liquid droplet. Right: a water droplet sliding at low angle of 7.5º. Corresponding advancing and receding contact angle on the PI/CA/F-PB-1/SNP-4 membranes measured to be about 162.1º and 155.7 º. Droplet sizes: ≈ 8 µL. b) Dynamic water repelling images (top) on the as-prepared membrane surface and time-lapse images of an oil droplet permeation (bottom) in the PI/CA/F-PB-1/SNP-4 surface.

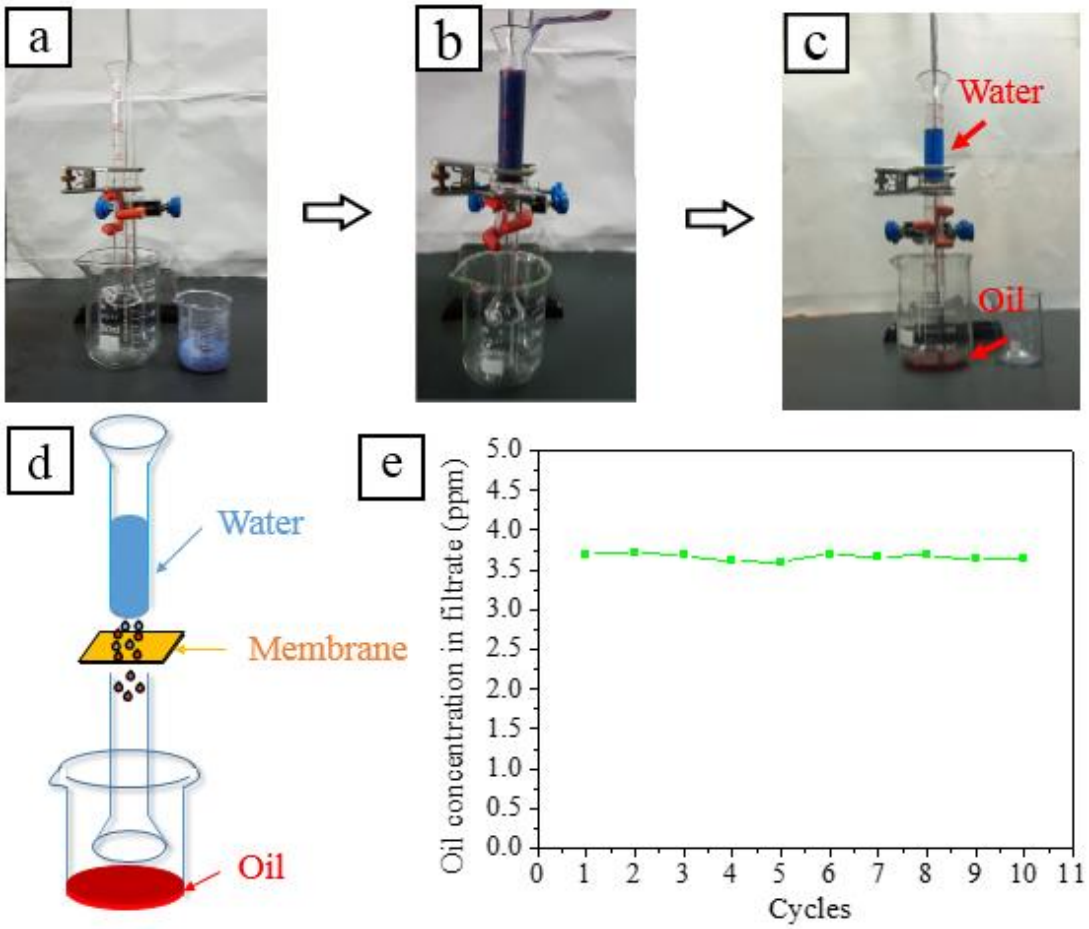

Fig. 10 Oil-water separation test. a) Separation apparatus with the oil-water mixture on top of an PI/CA/F-PB-1/SNP-4 nanofibrous membrane (without any further support); the water and oil were labeled using respectively methyl blue and oil red. b) The oil-water mixture was poured in the device. c) Oil passed through the membrane while water remained on top of the membrane. d) Schematic of oil-water separation setup. e) Oil concentration in the water fraction after separation for ten times cycles.

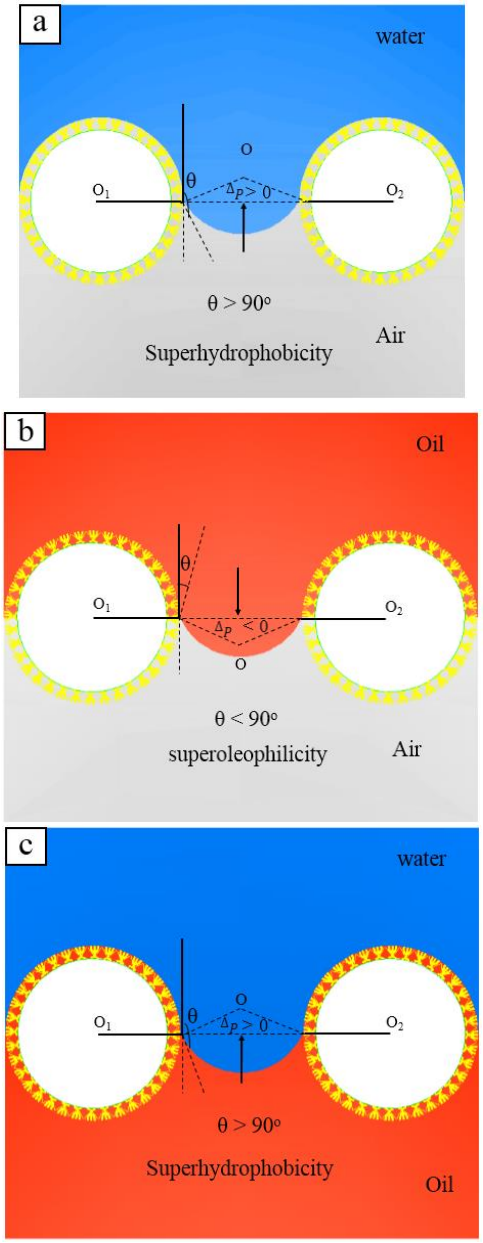

Fig. 11 Schematic diagrams of the liquid wetting model on the as-prepared PI/CA/F-PB-1/SNP-4 nanofibrous membrane. a) In air, the membrane shows superhydrophobicity that can sustain the water and permeable to oil, because $\Delta p > 0$. b) In air, the membrane displays superoleophilicity that oil can permeate the membrane, and it cannot support any pressure because $\Delta p < 0$. c) After oil permeation, some oil can be trapped among the interspaces between the PI/CA nanofibers and SNPs, thus the membrane shows superhydrophobicity, and water can be supported by the membrane, because $\Delta p > 0$. O is the center of the spherical of the meniscus; O_1 and O_2 are the cross-section center of the membrane. R is the curvature radius of the spherical of the meniscus.

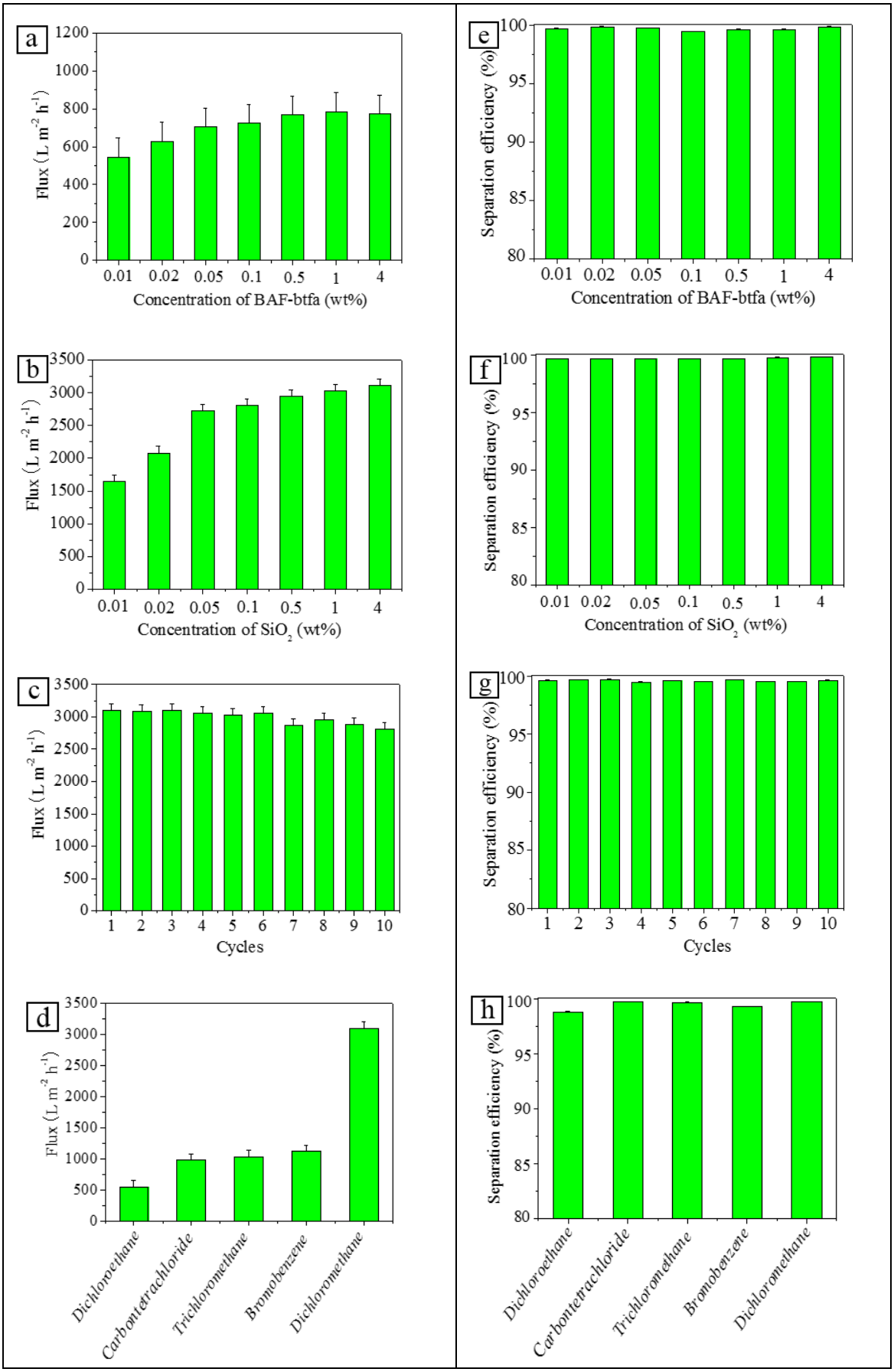
a
Flux (L m-2 h-1)
Concentration of BAF-btfa (wt%)
b
Flux (L m-2 h-1)
Concentration of SiO2 (wt%)
c
Flux (L m-2 h-1)
Cycles
d
Flux (L m-2 h-1)
Dichloroethane
Carbontetrachloride
Trichloromethane
Bromobenzene
Dichloromethane
e
Separation efficiency (%)
Concentration of BAF-btfa (wt%)
f
Separation efficiency (%)
Concentration of SiO2 (wt%)
g
Separation efficiency (%)
Cycles
h
Separation efficiency (%)
Dichloroethane
Carbontetrachloride
Trichloromethane
Bromobenzene
Dichloromethane

Fig. 12 (a-c) Flux of dichloromethane (DCM) through electrospun core/shell structured PI/CA nanofibrous membranes. (d) Flux of various oil-water mixtures through flexible PI/CA/F-PB-1/SNP-4 membranes. (e-g) Separation efficiency of the membranes for dichloromethane-water mixtures. (h) Separation efficiency of flexible PI/CA/F-PB-1/SNP-4 membranes for various oil-water mixtures. Experiments were performed in duplicate and repeated three times and the data are presented as mean ± SD (n = 3).

.

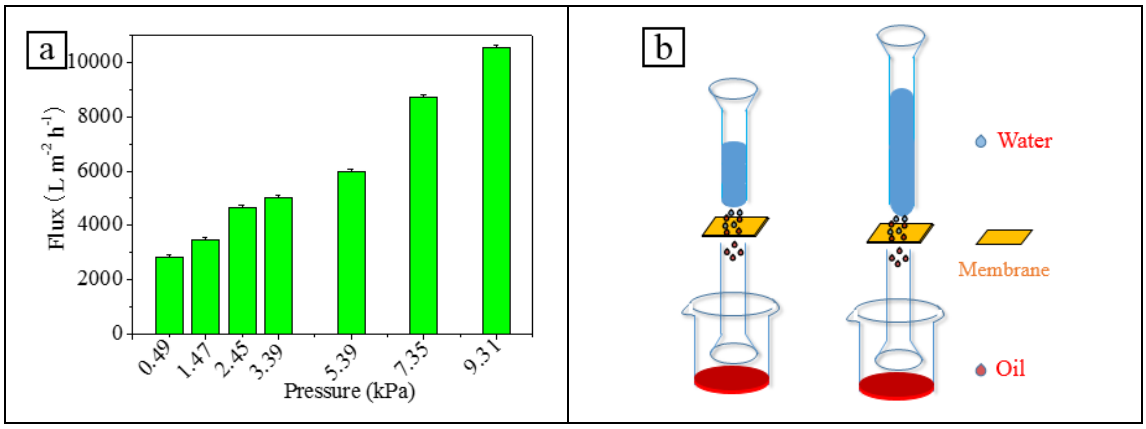

Fig.13 a) Flux of 10 mL DCM through PI/CA/F-PB-1/SNP-4 nanofibrous membranes with different height of glass tubes filled with oil and water. b) Schematic of (a). Experiments were performed in duplicate and repeated three times and the data are presented as mean ± SD (n = 3).

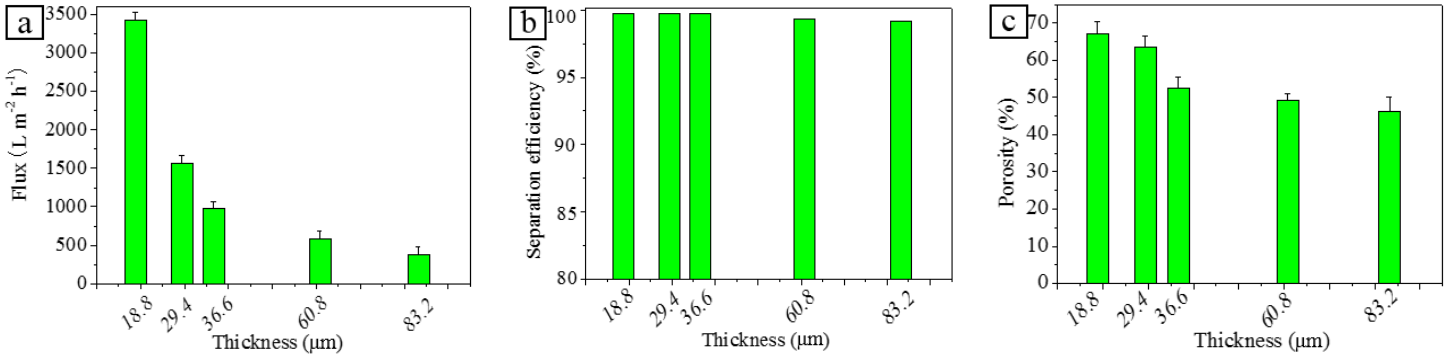

Fig. 14 a) Flux of DCM through PI/CA/F-PB-1/SNP-4 nanofibrous membranes with different thickness. b) Separation efficiency of these membranes for dichloromethane-water mixtures and their porosity (c). Experiments were performed in duplicate and repeated three times and the data are presented as mean ± SD (n = 3).

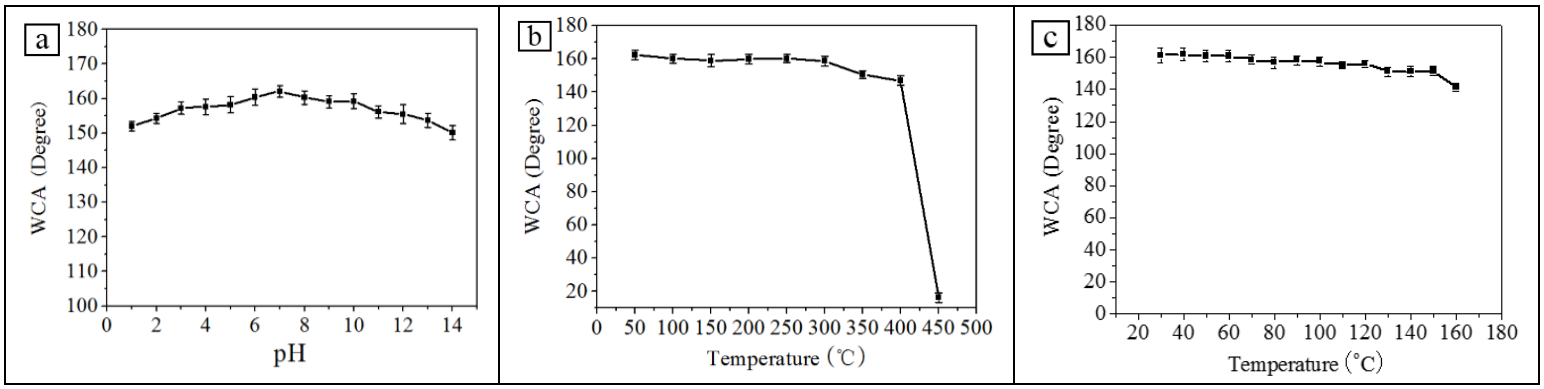

Fig.15 a) The relationship between pH and the WCAs of PI/CA/F-PB-1/SNP-4 nanofibrous membranes. b) WCA of the PI/CA/F-PB-1/SNP-4 nanofibrous membranes after calcination in air at different temperature for 10 min. c) WCA of the PI/CA/F-PB-1/SNP-4 nanofibrous membranes when heated in air at different temperature.